

Fischer–Tropsch Synthesis: Deactivation as a Function of Potassium Promoter Loading for Precipitated Iron Catalyst

Venkat Ramana Rao Pendyala · Uschi M. Graham · Gary Jacobs · Hussein H. Hamdeh · Burtron H. Davis

Received: 17 June 2014 / Accepted: 8 August 2014 / Published online: 23 August 2014
© Springer Science+Business Media New York 2014

Abstract The effect of potassium promoter loading (0, 0.5, 1.0 and 2.0 atomic ratio) on the performance of precipitated iron catalysts was investigated during Fischer–Tropsch synthesis using a continuously stirred tank reactor. Characterization by temperature-programmed reduction with CO, Mössbauer effect spectroscopy, and transmission/scanning transmission electron microscopy were used to study the effect of potassium promoter interactions on the carburization, phase transformation and carbon layer formation behavior of the catalysts. Under similar reaction conditions, all four catalysts exhibited similar initial CO conversions ($\sim 85\%$), whereas stability was found to increase with potassium loading up to 0.5 % (atomic ratio related to the iron), and further increases in potassium led to decreased activity. Unpromoted and excessively K loaded (2.0K/100Fe) catalysts exhibited similar deactivation trends with time and followed essentially similar conversion levels with time-on-stream. The selectivity of various potassium promoted catalysts was found to increase the average molecular weight of hydrocarbon products with increasing potassium loading. The deactivation rate was related to carbon deposition which could embed the iron carbide particles. If not enough K is present, Fe carbides tend to oxidize with TOS; with excessive K-loading, carbon deposition/site blocking become problematic.

Keywords Fischer–Tropsch synthesis · Iron catalyst · Potassium loading · Carbon layer formation · Mössbauer spectroscopy · Transmission electron microscopy

1 Introduction

Fischer–Tropsch synthesis (FTS) is a commercially proven and economically viable process for the production of hydrocarbon fuels from low value natural gas, coal, and biomass [1]. In the FTS reaction, synthesis gas produced from natural gas reforming or gasification of coal or biomass, and it is transformed to hydrocarbons in the presence of cobalt, ruthenium, or iron catalysts. With diminishing petroleum resources, increasing attention has focused on the FTS production of liquid fuels from these alternative energy sources. The product distribution is highly dependent on the process conditions and the type of catalyst used. Iron-based catalysts are very promising for FT processes because of their high activity and low cost. Furthermore, they are preferred for FT synthesis utilizing synthesis gas derived from coal or biomass owing to their intrinsic activity for the water gas shift (WGS) reaction, which allows the use of synthesis gas having low H_2/CO ratio (e.g., 0.7) directly, without the need for an upstream shift step.

Iron-based catalysts often contain small amounts of potassium and some other metals such as manganese, calcium, zinc, copper and magnesium as promoters to improve activity and selectivity [2]; the relatively stronger basicity of potassium influences the adsorption of reactants (CO and H_2) on the active sites. This leads to some effects on the FTS activity, an enhancement in the selectivity to olefins, the suppression of the formation of methane, and a selectivity shift to higher molecular weight products [3–5]. Nearly all iron-based FTS catalysts contain potassium as one of the

V. R. R. Pendyala · U. M. Graham · G. Jacobs · B. H. Davis (✉)
Center for Applied Energy Research, University of Kentucky,
2540 Research Park Dr., Lexington, KY 40511, USA
e-mail: burtron.davis@uky.edu

H. H. Hamdeh
Department of Physics, Wichita State University, Wichita,
KS 67260, USA

promoters, although the amount can vary depending on the desired product distribution. The overall effects of potassium on the behavior of iron-based FTS catalysts have been investigated over different catalyst systems [2–18]. Kölbl [3] examined the effect of potassium on the surface properties of supported iron and precipitated Fe–Cu–SiO₂ catalysts, and found that the addition of potassium on the precipitated iron catalyst enhanced CO chemisorption and suppressed H₂ chemisorption. The results were explained by the fact that potassium donates electrons to iron and facilitates CO chemisorption, since CO tends to accept electrons from iron (as described later in the discussion section). On the other hand, hydrogen with its higher surface coverage is inclined to donate electrons to iron, and the electrons donated to iron from potassium weaken the strength of the Fe–H bond. Hence, potassium strengthened the Fe–C bond and weakened the Fe–H bond [8, 10, 13, 19]. The results of Rankin and Bartholomew over Fe/SiO₂ catalyst indicated that the addition of potassium inhibits reduction of the catalyst [18]. Dry and Oosthuizen [7] have reported that the addition of potassium results in a decrease in the surface area of fused magnetite catalysts. In addition, the carbonization of iron during FTS proceeded more rapidly on potassium-promoted catalysts [5]. The effects of potassium on the FTS and WGS activities and product selectivity have also been investigated over a variety of iron-based catalysts [13, 17, 19, 20]. While some researchers have reported that FTS activity either increases [2, 6, 13] or passes through a maximum as a function of potassium loading [11, 20], others have found that potassium either has no effect on the activity for FTS [21] or suppresses it [17, 20]. In our previous study [22], we reported the activity/stability of an unpromoted and a 2 % potassium promoted iron catalyst during FTS, and the activities of these catalysts decreased in a similar manner with time on stream.

The activity of iron-based FTS catalysts changed during their operation because of sintering of metal particles, coke formation, poisoning and phase transformation [23, 24]. It is important in the design of iron-based FT catalysts to achieve a clear understanding of carbon deposition and phase transformations during different pretreatments and under industrial FTS conditions. Results of previous studies have shown that the formation of surface carbides is required before the catalyst can exhibit high activity [9, 17, 25]. It is well known that the distribution of iron phases in the catalyst changes with time-on-stream [22, 26]. The oxidation of the metallic iron and/or the iron carbide phases is believed to be one of the factors contributing to catalyst deactivation. Water (a primary product in the FTS reaction) and CO₂ (which is produced from the water–gas shift reaction) are usually considered to be oxidizing agents for iron phases [27, 28]. Apart from the oxidation of the iron phases, several authors have implicated a graphite-like

carbonaceous compound in the deactivation of iron catalysts [29, 30]. Coke formation from undesired side reactions affects the intrinsic activity through the coverage of sites and the blockage of pores [23, 24].

Structural (e.g., SiO₂) and chemical promoters (e.g., K and Cu) also influence FTS activity and selectivity. Yong et al. [31] reported that a potassium containing catalyst without SiO₂ addition possessed a markedly higher activity than catalysts containing SiO₂. The decreased activity with addition of SiO₂ was attributed by the authors to a decrease in the coordination of potassium due to the interaction between potassium and silica. Also, other chemical promoters (e.g., Cu), can facilitate reduction of Fe oxides at low temperature and improve the formation of the active phase for the FTS reaction [32]. These aspects are outside the scope of this work. The aim of the present study is to explore how the potassium loading influences the deactivation trends of unpromoted and K-promoted (i.e., containing variable concentrations of potassium) catalysts, and explain the reasons why the deactivation rate passes through a minimum with increasing K loading. FTS activity, selectivity and stability of a precipitated iron catalyst, without using any structural or other chemical promoters, were investigated as a function of potassium promoter loading.

2 Experimental

2.1 Catalyst Preparation

The precipitated iron catalyst parent batch was prepared by using a ferric nitrate solution obtained by dissolving iron (III) nitrate nonahydrate (1.17 M) in deionized water. A controlled flow of the iron nitrate mixture was added to the precipitation vessel together with a stream of ammonium hydroxide (14.8 M) that was added at a rate to maintain a pH of 9.0. The slurry was recovered using a vacuum filter and the solids were washed twice with deionized water. The final filter cake was dried for 24 h in an oven at 110 °C with flowing air. For this study, the iron catalyst base powder was then impregnated with varying amounts of aqueous potassium nitrate solution to produce a desired composition of Fe:K = 100:0.5, 100:1.0, and 100:2.0 (atomic ratios). Catalysts were then dried at 110 °C overnight, followed by calcination at 350 °C in flowing air for 4 h.

2.2 Catalyst Characterization

2.2.1 Surface Area and Pore Size Distribution

The measurement of BET surface area and porosity of the calcined catalysts was conducted using a Micromeritics

Tri-Star system. Before performing the test, the temperature was gradually ramped to 160 °C and the sample was evacuated at least 12 h to approximately 50 mTorr. The BET surface area, pore volume (single point), and average pore radius (single point) were obtained for each sample.

2.2.2 Temperature Programmed Reduction (TPR) of CO

Temperature programmed reduction (TPR) of CO profiles of calcined catalysts were recorded using a Zeton-Altamira AMI-200 unit equipped with a thermal conductivity detector (TCD). The TPR was performed using a 10 % CO/He gas mixture (referenced to helium) at a flow rate of 30 cm³/min. The catalyst samples were heated from 50 to 525 °C using a heating ramp rate of 10 °C/min and held for 1 h. A liquid-nitrogen trap was used to continuously remove the CO₂ produced.

2.2.3 Morphology and Phase Transformation by HRTEM and STEM

The morphology and phase transformations of individual catalyst particles were analyzed by transmission electron microscopy (TEM). Samples were prepared on TEM copper grids (200 mesh) from representative catalyst powders after FTS and removal of residual FT products. TEM imaging was performed using a JEOL 2010F field-emission gun transmission electron microscope (accelerating voltage of 200 keV and magnification ranging from 50 to 1,000 K). Images were recorded with a Gatan Ultrascan 4 k × 4 k CCD camera and all data processing and analysis applied the Gatan Digital Micrograph software. Furthermore, scanning transmission electron microscopy (STEM) imaging was performed with a high angle annular dark field (HAADF) detector that was also used with a Gatan imaging filter. This allowed the imaging of only the catalyst particles while excluding the carbon deposits since the light elements were not detected in HAADF. This provides an excellent contrast in the TEM and STEM images that reveal the carbon deposits.

2.2.4 Mössbauer Spectroscopy

Mössbauer spectra were collected in transmission mode by a standard constant acceleration spectrometer (MS-1200, Ranger Scientific). A radiation source of 30 mCi ⁵⁷Co in Rh matrix was used and spectra were obtained using a gas detector. The catalyst samples collected from the CSTR were dispersed in the re wax and present as a solid phase at room temperature. For the low temperature measurements, the samples were placed inside a vibration free closed cycle cryostat (Cryo-Industries of America). Structural analysis of the samples was performed by least-squares fitting of the

Mössbauer spectra to a summation of hyperfine sextets. The least squares fitting procedure employed user defined functions within the PeakFit program. The parameters for each sextet in the fit consisted of the position, width and height of the first peak, the hyperfine magnetic field, and the quadrupole electric field. These parameters were allowed to vary freely to obtain the best fit of the experimental data. Errors in the determined percentages for the Fe values are about ±3 % for well resolved spectra; in those that contain several iron oxide and carbide phases, the uncertainty increased with the complexity of the representative spectrum (i.e., depending on the degree of overlap and the weakness of the signal). However, these complex spectra were obtained during the course of transformation from a predominantly iron oxide form to an iron carbide/oxide mixture and conform to a general trend.

2.3 Catalyst Testing

The FTS experiments were conducted in a 1 L CSTR equipped with a magnetically driven stirrer with turbine impeller, a gas-inlet and a vapor outlet line, and a SS-fritted filter (2 micron) placed external to the reactor. A tube fitted with a SS-fritted filter (0.5 micron opening) extended below the liquid level of the reactor and was used to withdraw reactor wax in order to maintain a nearly constant liquid level in the reactor. Another SS dip-tube (1/8" OD) extended to the bottom of the reactor and was used to withdraw aliquots of the catalyst/wax slurry from the reactor at different synthesis times. Separate mass flow controllers were used to regulate the flow of hydrogen and carbon monoxide at the desired rate. The gases were pre-mixed in a mixing vessel before entering the reactor. Carbon monoxide was passed through a vessel containing lead oxide-alumina to remove traces of iron carbonyls. The mixed gases entered the CSTR below the stirrer that was operated at 750 rpm. The reactor slurry temperature was maintained constant (±1 °C) by a temperature controller.

Catalyst (15 g) was added to C₃₀ oil (310 g) in the CSTR to produce a slurry that contained about 5 % iron oxide. The reactor temperature was then raised to 270 °C at a rate of 1 °C/min. The catalyst was activated using CO at a space velocity of 3.0 sl/h/g_{cat} at 270 °C and 175 psig for 24 h. At the end of the activation period, a sample of activated catalyst (Sample # 1) was withdrawn via the slurry withdrawal dip-tube of the CSTR. The FTS reaction was then started by adding the synthesis gas mixture to the reactor at a space velocity of 3.0 sl/h/g_{cat} and a H₂/CO ratio of 0.7. The conversions of CO and H₂ were obtained by gas-chromatography analysis (micro-GC equipped with TCDs) of the reactor exit gas mixture. The reaction products were collected in three traps maintained at different

temperatures: a hot trap (200 °C), a warm trap (100 °C) and a cold trap (0 °C). The products were separated into different fractions (rewax, wax, oil and aqueous phase) for quantification. However, the oil and the wax fractions were mixed prior to GC analysis.

Catalyst/rewax slurry was withdrawn at different reaction times via the dip-tube after sufficient purging. In a typical catalyst slurry sampling procedure, about 30 g of catalyst slurry was purged and then 1 g of catalyst slurry was collected as a representative sample from the reactor at that time. To prevent changes in catalyst electronic and geometric structure, during sampling and removal of wax products, catalyst was removed in a sampling bottle containing inert gas, and the sample was transferred to an air-free environment (inert chamber); moreover, the typical Soxhlet extraction procedure was avoided. Instead, the withdrawn sample was diluted with hot (about 70 °C) ortho-xylene to remove the high molecular weight FT-wax fractions. It was not possible to completely remove the FT-wax from the catalyst particles by this method. However, the remaining wax acts as a protective cover for the air-sensitive catalyst particles.

3 Results

BET surface area and pore size distribution results of unpromoted and various potassium promoter loaded iron catalysts are shown in Table 1. The surface areas for the potassium promoted catalysts were found to be lower than the unpromoted catalyst, which has an area of 43.2 m²/g. With increasing potassium loading, the surface areas of the catalysts were found to decrease. For the potassium promoted catalysts, if the promoter oxide does not contribute to the surface area, the corrected surface area would have been higher than the obtained values listed in Table 1. These values indicate that there is some pore blockage in the promoted catalysts and this is likely due to the promoter oxide clusters blocking a fraction of pores from the adsorbing gas or in decreasing the porosity during the second drying step. For the potassium promoted catalysts, the average pore size shifts to higher values, suggesting that the smaller pores are blocked and/or destroyed in comparison to the unpromoted catalyst.

Table 1 BET surface area and pore size distribution results of various potassium loaded iron catalysts

Catalyst	BET surface area (m ² /g)	Single point pore volume (cm ³ /g)	Average pore radius (nm)
100Fe:0.0K	43.2	0.203	9.4
100Fe:0.5K	40.2	0.210	10.4
100Fe:1.0K	39.8	0.212	10.7
100Fe:2.0K	29.8	0.199	13.4

Temperature-programmed reduction with CO (CO-TPR) was used to investigate the carburization behavior of catalysts in flowing CO. The CO-TPR profiles of various potassium promoter loaded iron catalysts are shown in Fig. 1. The profiles show two apparent reduction/carburization peaks. Actually, a very weak peak before 240 °C is also detected, which could be ascribed to the reduction of hematite (α -Fe₂O₃) to magnetite (Fe₃O₄) and the first major peak is located in the temperature range of 240–300 °C. These peaks are associated with reduction of Fe₂O₃ to lower oxides (i.e., Fe₃O₄ and defect-laden form of this oxide) prior to carburization. The peaks are fully consistent with our previous CO-TPR XANES/EXAFS studies [33–35]. The second peak is located in the temperature range of 350–525 °C. This could be ascribed to the carburization of iron oxides [36–38]. Primarily the second main peak is significantly affected by the potassium promoter loading, where the carburization rate is more rapid, and the peak maximum is shifted to slightly lower temperature with increasing potassium loading. These results clearly reveal that the loading of the potassium promoter has a significant effect on the carburization rates of iron catalysts.

The CO conversion levels for the unpromoted and various potassium promoter loaded iron catalysts are shown in Fig. 2. To maintain experimental control, similar activation and reaction conditions were maintained for all catalysts. Unpromoted and various potassium loaded catalysts exhibited high initial CO conversions, and all catalysts showed similar initial CO conversions (~85 %). The stability of the catalysts increased significantly with the addition of potassium promoter to the iron catalysts, passing through a maximum at a potassium content of about 0.5 %. Beyond this potassium concentration, with increasing potassium loading a decrease in catalyst activity/stability was observed with time on stream. The 100Fe:2.0K catalyst displayed a similar initially high

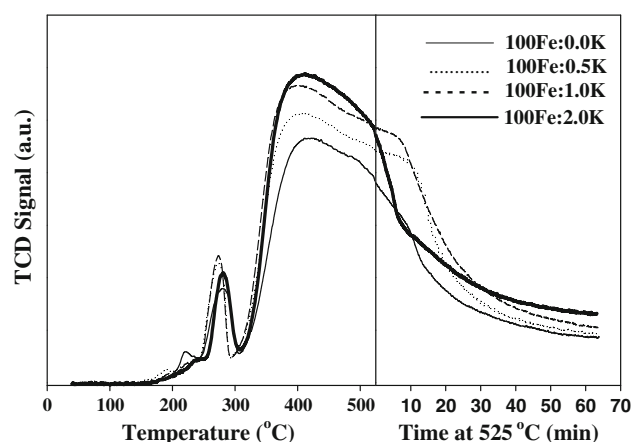


Fig. 1 CO-TPR profiles various potassium promoter loaded iron catalysts

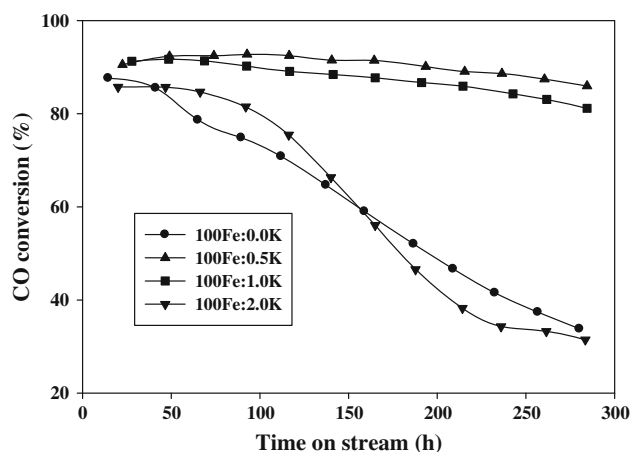


Fig. 2 CO conversion against time-on-stream for various potassium promoter loaded iron catalysts ($T = 270\text{ }^{\circ}\text{C}$, $P = 13\text{ atm}$, $\text{H}_2/\text{CO} = 0.7$, $\text{SV} = 3\text{ SL/g}_{\text{catalyst}}/\text{h}$)

activity like the other catalysts, but the activity decreased significantly with time on stream and conversions were comparable to the unpromoted catalyst. For the characterization (Mössbauer and TEM) studies, a total of three catalyst slurry samples were collected during CSTR tests of the unpromoted and various potassium loaded catalysts—one sample after carburization and an additional two samples during FTS (one at the middle of the run and another at the end of the run). Generally, CO conversion will decrease immediately following withdrawal of the catalyst sample from the reactor because the space velocity is increased per gram of the catalyst remaining in the reactor. To avoid that change in conversion, the amount of catalyst that was withdrawn from the reactor was subtracted and the space velocity was adjusted to maintain similar conditions (conversion, partial pressures of CO and hydrogen per gram of catalyst). The amount of catalyst withdrawn from the reactor was determined based on the amount of accumulated re wax and the amount of catalyst loaded in the reactor; the percentage of error range was ± 5 .

Mössbauer effect spectroscopy is a useful technique that can provide quantitative information on the fractions of various iron phases present in the catalyst samples [22]. The iron phase composition of unpromoted and various potassium promoter loaded iron catalysts, after carburization and during FTS, as determined by fitting the Mössbauer spectra at 20 K measurements, are listed in Table 2. Although the FTS reaction does not occur in the bulk phase of carbides, the carbides can have FTS-active sites on their surfaces. Thus, it is proposed that iron carbides are the main active phases for the FTS reaction [17, 39–42], and

Table 2 Summary of phase identification of iron from Mössbauer spectroscopy analysis for various potassium loaded iron catalyst

Catalyst	FT synthesis time (h)	Fraction of Fe at 20 K (%)		
		Fe_3O_4	$\delta\text{-Fe}_{2,2}\text{C}$	$\chi\text{-Fe}_5\text{C}_2$
100Fe:0.0K	0	7	21	72
	42	38	3	59
	281	85	0	15
100Fe:0.5K	0	17	0	83
	96	32	0	68
	285	40	0	60
100Fe:1.0K	0	11	7	82
	95	25	21	54
	285	23	44	33
100Fe:2.0K	0	19	8	73
	117	19	58	23
	284	7	88	5

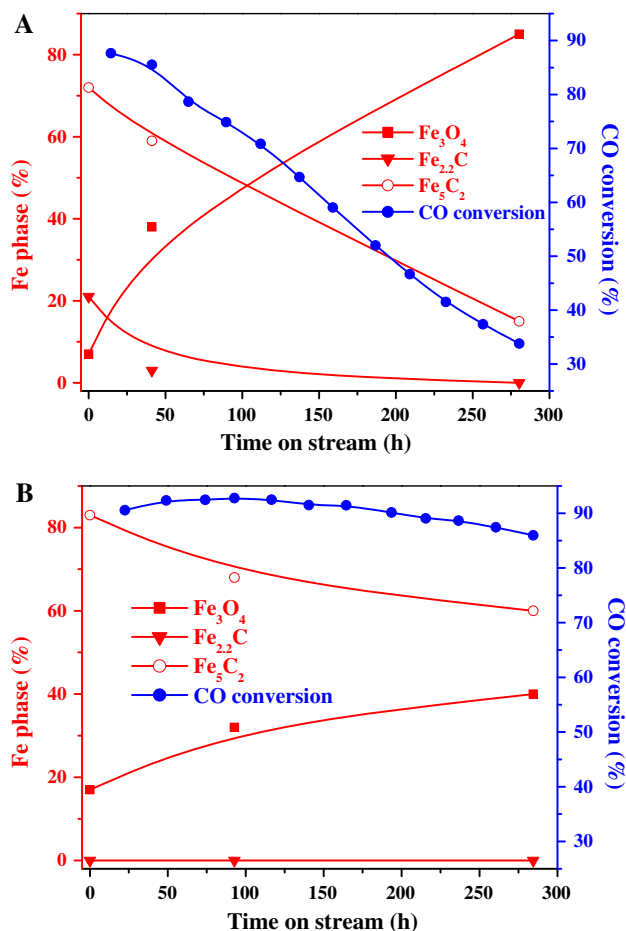


Fig. 3 The change in distribution of the iron phases on CO conversion **a** unpromoted iron catalyst; **b** 0.5% K promoted iron catalyst

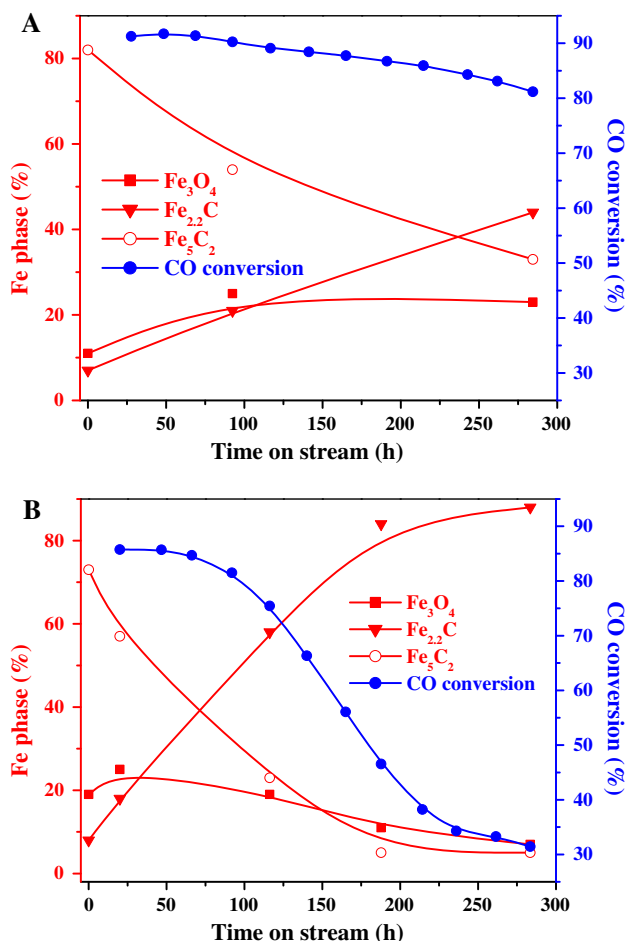


Fig. 4 The change in distribution of the iron phases on CO conversion **a** 1.0 % K promoted iron catalyst; **b** 2.0 % K promoted iron catalyst

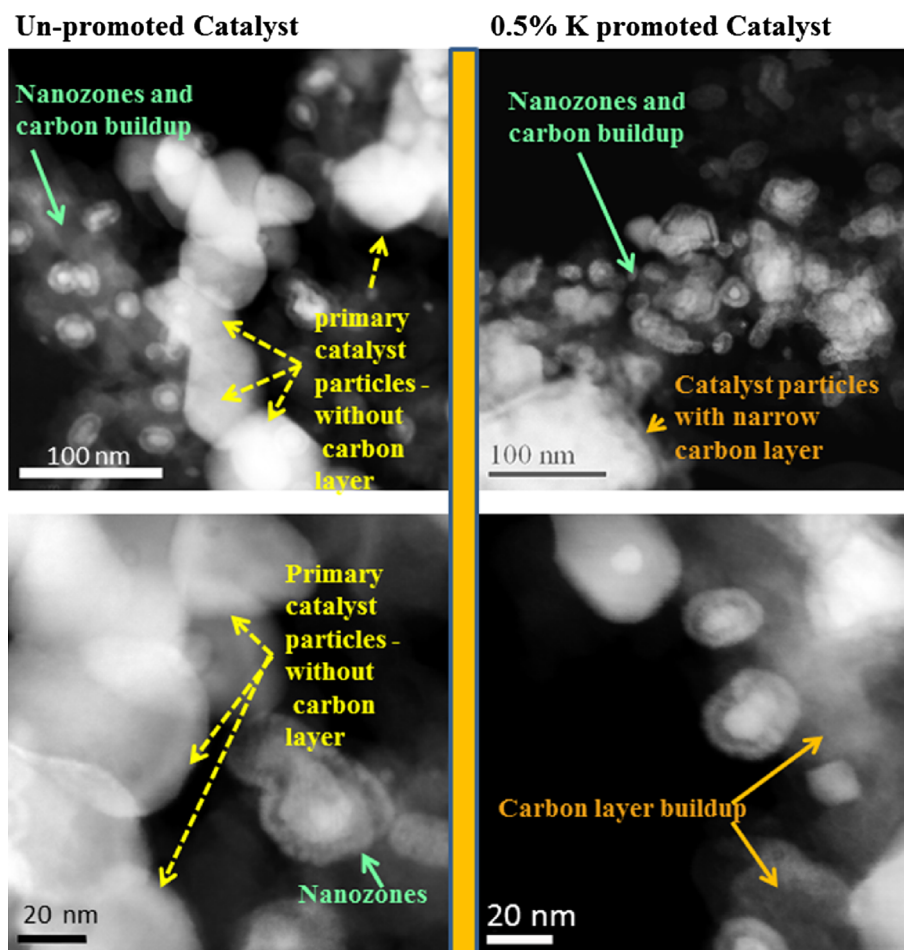
their content can be used to monitor the formation of FTS active sites. At the end of a 24 h activation period for the unpromoted iron catalyst, low temperature Mössbauer results reveal that the initial hematite converted to a mixture of 72 % χ -Fe₅C₂, 21 % δ -Fe_{2.2}C and 7 % Fe₃O₄ and that the potassium promoted catalysts had a similar content of iron carbide (χ -Fe₅C₂) phase after the 24 h activation period. Figure 3a represents the effect of the changing distribution of iron phases on CO conversion for an unpromoted catalyst. The catalytic activity showed a gradual decrease with time and the deactivation rate was found to be 4.86 % per day. The iron carbide phase gradually decreased while the corresponding oxide (Fe₃O₄) phase increased with time. The CO conversion followed a similar trend as the excessively K-loaded (2.0 K) catalyst but deactivated slightly more rapidly.

Figure 3b shows the changing distribution of the iron phases on CO conversion for the 0.5 K promoted iron catalyst. CO conversion was found to be stable during about 125 h on stream and after that slightly decreased

with time and the observed rate of deactivation was 0.58 % per day. The iron carbide χ -Fe₅C₂ phase decreased with time from 83 % to only 60 % and the formation of δ -Fe_{2.2}C phase was not observed, whereas the corresponding Fe₃O₄ phase increased with time from 17 to 40 %. Figure 4a shows the changing distribution of the iron phases on CO conversion for the 1.0 K promoted iron catalyst. CO conversion was found to be stable during about 60 h on stream and after that slightly decreased with time on stream; the deactivation rate was found to 0.94 % per day. The iron carbide χ -Fe₅C₂ phase decreased with time from 83 to 33 % and the corresponding of δ -Fe_{2.2}C phase gradually increased from 7 to 44 %, whereas the corresponding Fe₃O₄ phase also slightly increased with time from 11 to 23 %. Figure 4b shows the changing distribution of the iron phases on CO conversion for the 2.0 K promoted iron catalyst. CO conversion was found to gradually decrease with time and the loss of CO conversion was found to be 5.11 % per day. The iron carbide χ -Fe₅C₂ phase gradually decreased with time from 73 to 5 % and the corresponding δ -Fe_{2.2}C phase increased from 8 to 88 %, whereas the Fe₃O₄ phase remained virtually unchanged or perhaps slightly decreased with time. For the 2.0 K promoted catalyst, the rate of in situ regeneration by re-carburization is deemed to be high. Also, Mössbauer spectra of samples revealed that the δ -Fe_{2.2}C fraction had gradually increased with time.

A TEM/STEM study was carried out to examine the morphological effects caused by the K promoter on the catalysts after FTS in a CSTR to compare the location and buildup of amorphous carbon deposits on the surfaces of the catalyst grains. The TEM/STEM investigation showed that the un-promoted catalyst had many primary catalyst particles that did not show any carbon buildup and amorphous carbon was observed in close proximity to catalyst grains that show nanozones (carbide core and outer iron oxide layer with a rim of carbon buildup at the surface (Fig. 5)). In contrast, the potassium promoted catalysts showed increased amorphous carbon buildup with an increase in potassium promoter loading (Figs. 5, 6). With an increase in K-promoter loading the catalyst also shows a general trend of increased particle size for both poly crystals and nanozones. The 1.0 % K-promoted catalyst was unique in that it had a bimodal particle size distribution. By comparison, the 2.0 % K-promoted catalyst had much larger nanozones and also larger poly crystals and more amorphous carbon (Fig. 6). The TEM imaging helped greatly to observe differences in the amorphous carbon buildup and location among the un-promoted and K-promoted catalysts and the variances are illustrated in Fig. 7. Most importantly, carbon layer formation around catalyst grains increases with increasing K-loading both in its selectivity towards individual grains and in its layer

Fig. 5 STEM images at two different magnifications of unpromoted and 0.5 % K-promoted iron catalysts

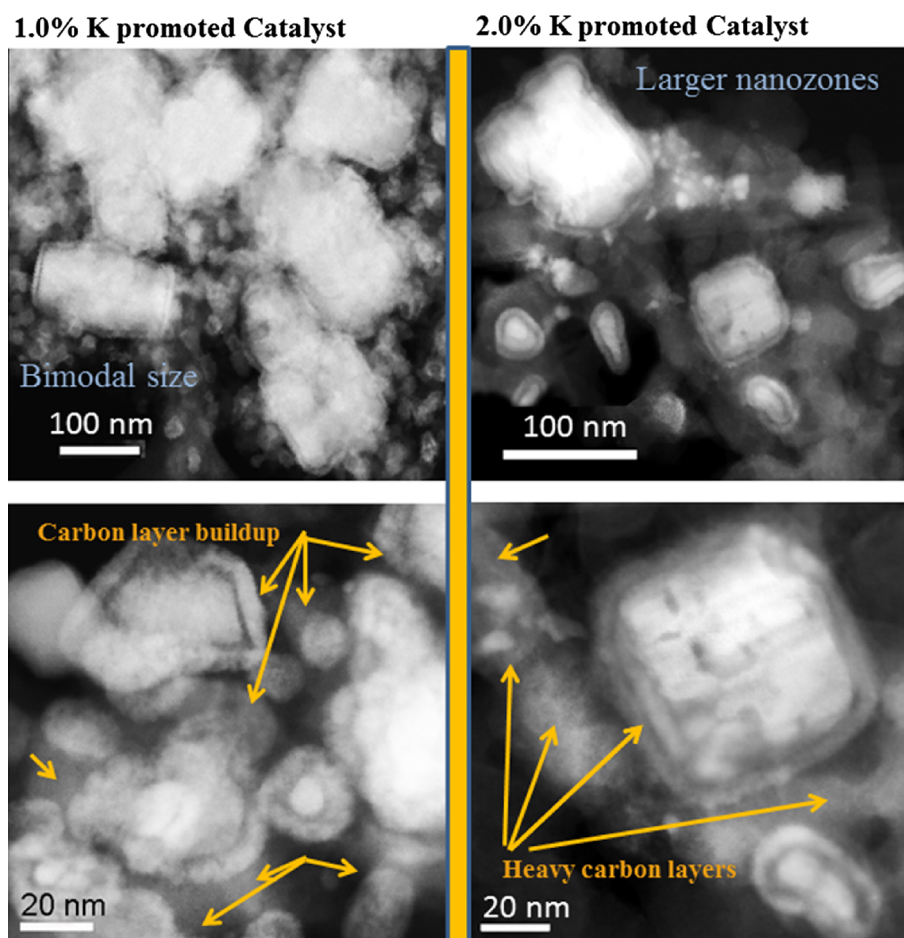


thickness. On the other hand, carbon buildup in the unpromoted catalyst occurs more randomly and primarily with nanozones and seems to leave primary catalyst grains uncoated. The schematic in Fig. 8 shows a side-by-side comparison of the relative degree of carbon buildup and also locations of carbon deposits for the four catalysts used. Differences in the degree of carbon buildup for unpromoted versus K-promoted catalysts after FT synthesis were observed in conjunction with differences in the location of amorphous carbon. While the unpromoted catalyst had the smallest particle size range (many primary catalyst particles without nanozones) and a more random buildup of amorphous carbon, the K-promoted catalysts had a bimodal particle size range for the 0.5 and 1.0 % potassium promoted catalysts and at higher K-loading (2.0 %), mainly large poly-crystals and large nanozones remained. The highest potassium loading led to the greatest amount of carbon being deposited on the catalyst surface.

The catalyst samples that were analyzed using TEM/STEM represent the catalyst particles after FTS samples were withdrawn from the reactor before the end-of-run. With the exception of distinct layers of amorphous carbon,

the used catalyst particles are polycrystalline. The catalyst particles usually include numerous crystallites arranged in layers and make up individual nanozones in the used catalyst grains, as shown in Figs. 5, 6 and 7. Primary catalyst particle size before FT synthesis was typically observed to be ~ 5 nm and can range from 5 to 20 nm. The degree of particle growth after FT synthesis appears to be governed by the amount of potassium used as promoter. Specifically, the unpromoted catalyst had the smallest particle size increase after FT while the 2.0 % K promoted catalyst had the highest degree of particle size growth. It is important to point out that only a fraction of the catalyst grains in any of the samples of the 0.5, 1.0 and 2.0 % K promoted catalyst samples increased in size and all samples showed a broad size range from 5 to 150 nm. However, when comparing the samples, the higher potassium loading led to a higher degree of particle size growth. It was also observed that the 1.0 % K promoted sample after FT synthesis had a bimodal size distribution with particles either in the ~ 5 –10 nm size range or in the 50–150 nm size range. This indicates a particle size growth that is ~ 10 times that of the primary catalyst grains.

Fig. 6 STEM images at two different magnifications of 1.0 % K-promoted and 2.0 % K-promoted iron catalysts



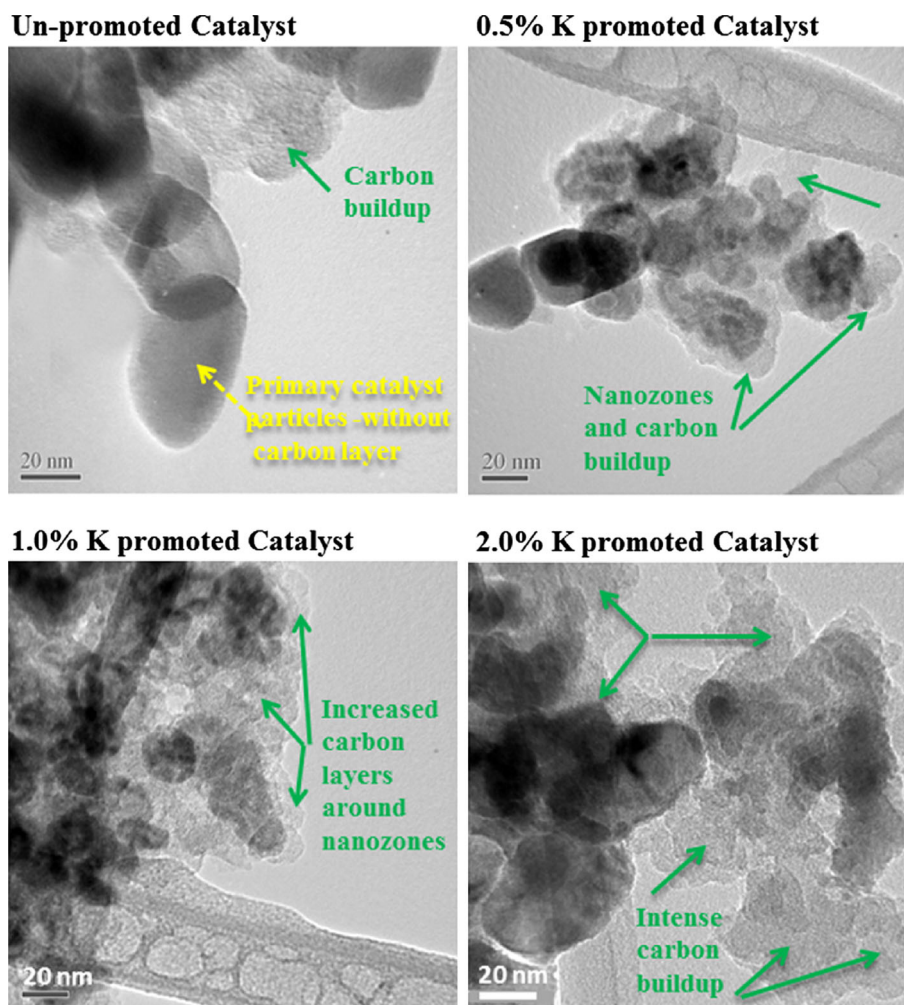
The effect of potassium promoter loading on the product selectivities of iron catalysts is shown in Table 3. In FT synthesis, it is known that the conversion level influences the selectivity, in part due to increasing partial pressure of water [43, 44] and by decreasing the partial pressure of reactants. It is therefore important to compare the catalysts at a similar CO conversion level. Experiments were run with the iron catalyst at a constant conversion of CO of ca. 55 %. With increasing the potassium loading, the selectivities of light hydrocarbons (methane and C₂–C₄) were lower and the corresponding higher hydrocarbon (C₅+) selectivities increased. Carbon dioxide selectivity was also found to increase with increasing potassium loading. Table 3 shows that the average molecular weight of hydrocarbon products increases with increasing potassium loading relative to the unpromoted catalyst. The increase in average molecular weight of hydrocarbon products is likely due to an enhancement of CO and suppression of H₂ surface coverage in the presence of potassium. Since chain termination results from the hydrogenation of the iron-carbon bond, the presence of potassium enhances the probability of continued chain growth, i.e., formation of higher molecular weight

products [3, 8, 13]. As can be seen in Table 3, the chain growth probability (α) increased with increases in potassium loading. The olefin/paraffin ratios as a function of carbon number for various potassium promoted iron catalysts are shown in Fig. 9. The olefin content increases from C₂ to C₃/C₄, reaches a maximum value, and then decreases with increasing carbon number. Ethene is the most reactive olefin with respect to hydrogenation, and its selectivity is lower than that of C₃ and C₄ olefins, whereas the increase in hydrogenation activity (i.e., lower olefin content) of higher molecular weight olefins may be attributed to their increased reactivity, to a greater absorption of long chain molecules and, more likely, to their longer retention time in the reactor. Olefin to paraffin ratio was found to increase with increasing potassium promoter loading as potassium promotion suppresses the secondary hydrogenation of olefins.

4 Discussion

It is well known that potassium is used as a chemical promoter in iron-based catalysts. Since potassium is

Fig. 7 TEM images of un-promoted and potassium promoted iron catalysts compared at similar magnification (20 nm). Carbon buildup is indicated with *arrows*



assumed to donate electron to the vacant d orbital of the transition metal as evidenced by the lowering of the metal work function [45], its presence would enhance the dissociative adsorption of CO, while suppressing H₂ adsorption [12, 45, 46]. Therefore, potassium facilitates the carburization of catalysts in CO [8, 46, 47] as demonstrated by the lower temperatures and faster rates observed in Fig. 1. These results are in good agreement with previous studies of potassium promoted iron catalysts [12, 48].

A large number of studies have been performed to investigate the effect of potassium on the FTS activity over various iron-based catalysts under different reaction conditions [2, 3, 6, 11–13, 17, 19, 20]. It was reported that FTS activity can either increase or decrease with an increase in potassium loading; some researchers have found that it passes through a maximum as a function of potassium content, or even that it has no direct relationship with potassium level. Anderson [2] found, however, that the activity of potassium promoted alumina supported iron catalyst was even lower than that of un-promoted catalysts. Bukur et al. [13] found that potassium significantly

improved FTS activity within the range of 0–0.5K/100Fe, but beyond this concentration the effect of promotion was negligible. Kölbel [3] postulated that the reduced catalysts containing potassium had a higher concentration of active sites than with un-promoted catalyst, and therefore accelerated the FTS activity. With further increases in the potassium content, the active sites may be blocked by potassium, resulting in a decline in catalyst activity. Furthermore, as stated earlier, the addition of potassium is in favor of carbon deposition on the surface, which leads to the formation of inactive carbon covering the active sites on the surface and thus leads to a further decline in the FTS activity [6, 19]. The effect of potassium promoter loading on FTS activity/stability observed in the present study passes through a maximum at 0.5K/100Fe, and further increases in potassium loading increased the deactivation rate.

In the present study, all of the catalysts exhibited high initial activity, but the activity was found to decrease with time on stream. The rate of deactivation was low for the 100Fe:0.5K catalyst, and the deactivation rates were similar for the unpromoted and 100Fe:2.0K catalysts

Fig. 8 Schematic representation of the carbon buildup for un-promoted and K-promoted iron catalysts after FT synthesis

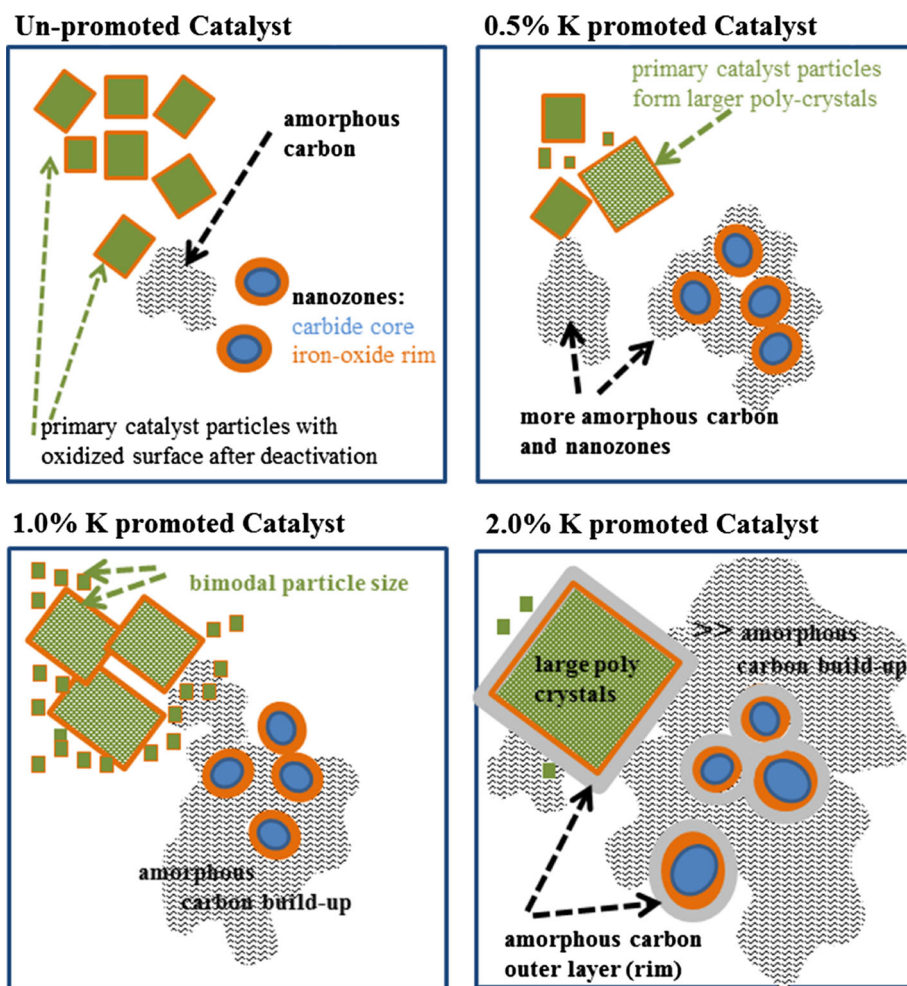


Table 3 Effect of product selectivity for various potassium loaded iron catalysts

Catalyst	Deactivation rate per day (%)	CO conversion (%)	CO ₂ selectivity (%)	Selectivity _{CO₂ free} (%)			Chain growth probability (α)
				C ₁	C ₂₋₄	C ₅₊	
100Fe:0.0K	4.86	59.0	41.4	6.2	25.1	68.7	0.83
100Fe:0.5K	0.58	57.3	44.6	5.2	23.1	71.7	0.84
100Fe:1.0K	0.94	55.6	47.9	4.5	20.3	75.2	0.88
100Fe:2.0K	5.11	56.1	48.1	3.0	12.5	84.5	0.91

(Reaction conditions: T = 270 °C, P = 13 atm, H₂/CO = 0.7)

(Table 3). Deactivation rates were observed to increase according to the following trend: 100Fe:0.5K < 100Fe:1.0K < << 100Fe < 100Fe:2.0K. Deactivation of the iron catalysts may be explained by the following four mechanisms, which have been described in the literature. Those are: (1) active iron carbide phases are gradually oxidized to magnetite (Fe₃O₄), which is relatively inactive for FTS [28, 49, 50]; (2) deposition of inactive carbonaceous compounds takes place on the surface of the catalyst, thereby limiting the contact between reactant gases and the catalytically active phase [17, 29, 51–53]; (3) sintering,

which is the loss of catalytic surface area due to ripening or migration and coalescence of iron phases [54, 55]; and (4) poisoning and deactivation by sulfur compounds, which are typically present in most syngas feeds. In the present study, the same syngas was used from two pure H₂ and CO tube trailers and so the possibility of poisoning by sulfur compounds was ruled out. For the unpromoted iron catalyst, Mössbauer results indicate that the iron carbide phase (χ-Fe₅C₂) gradually decreased while the corresponding oxide (Fe₃O₄) phase increased with time (Table 2). The decrease in CO conversion (Fig. 2) for the unpromoted catalyst can

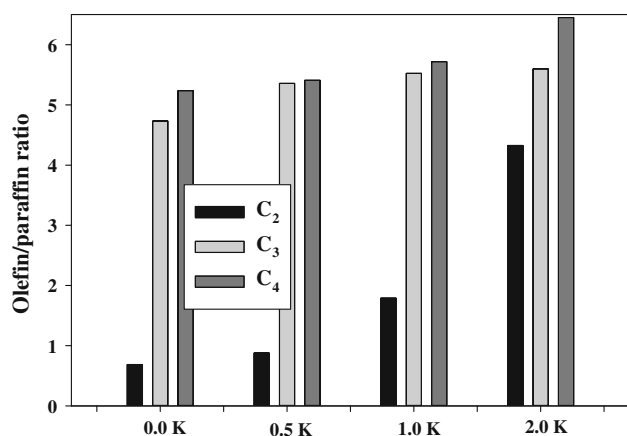


Fig. 9 Olefin/paraffin ratios for various potassium promoted iron catalysts ($T = 270\text{ }^{\circ}\text{C}$, $P = 13\text{ atm}$, $\text{H}_2/\text{CO} = 0.7$, CO conversion $\sim 55\%$)

be explained by the gradual increase in the inactive Fe_3O_4 phase that forms as a result of the oxidation of the catalyst. TEM results of the unpromoted catalyst showed that the formation of a carbonaceous layer on the catalyst surface was very small. Our previous study [56] on the effect of water co-feeding to an iron-based FT catalyst (promoted with silica, potassium, and copper) showed that the effect of water was very sensitive to the reaction temperature. At high temperatures ($270\text{ }^{\circ}\text{C}$), the co-feeding of 10 % water at a CO conversion level of about 50 % resulted in increased WGS activity, leaving the FT activity virtually constant. However, at $230\text{ }^{\circ}\text{C}$, the total CO conversion was depressed drastically and irreversibly. This deactivation was related to the oxidation of the iron carbide to magnetite; Mössbauer results further confirm this oxidation. In this study, even though the reaction was carried out at $270\text{ }^{\circ}\text{C}$, the present catalyst did not contain any structural or chemical promoters. The observed deactivation is likely due to the water produced during FTS oxidizing the iron carbides of the unpromoted iron catalyst [27, 28, 57].

For the 100Fe:0.5K catalyst the activity was stable until $\sim 200\text{ h}$ on stream, and after that it slightly decreased with time; the deactivation rate was low at 0.8 % per day. Mössbauer results showed that the iron carbide phase ($\chi\text{-Fe}_5\text{C}_2$) slightly decreased from 83 to 60 %, while the corresponding oxide (Fe_3O_4) phase slightly increased from 17 % to only 40 % even after $\sim 280\text{ h}$ on stream. Slight deactivation after 200 h TOS might be due to some extent of oxidation of the catalyst because this catalyst did not contain other chemical promoters (e.g., Cu). TEM results of the 0.5K/100Fe catalyst showed that the formation of a carbonaceous layer on the catalyst surface was very small. For the 100Fe:1.0K catalyst, the activity was slightly less stable and the deactivation rate was 0.9 % per day. Mössbauer results indicated that the iron carbide phase ($\chi\text{-}$

Fe_5C_2) gradually decreased from 82 to 33 %, and the corresponding $\text{Fe}_{2.2}\text{C}$ phase increased from 7 to 44 %, while growth of the oxide (Fe_3O_4) phase was similar (11–23 %) during $\sim 280\text{ h}$ on stream. TEM results of the 1.0K/100Fe catalyst showed that the formation of the carbonaceous layer on the catalyst surface was slightly higher. The primary route of catalyst deactivation may be carbon deposition on the surface of the catalyst.

With the 100Fe:2.0K catalyst, the iron carbide $\chi\text{-Fe}_5\text{C}_2$ phase gradually decreased with time and the corresponding $\delta\text{-Fe}_{2.2}\text{C}$ phase increased, whereas the Fe_3O_4 phase remained virtually unchanged or perhaps slightly decreased with time. Therefore, the deactivation could not be explained by the oxidation process as was the case for the unpromoted catalyst, since the fraction of the Fe_3O_4 phase remained nearly the same. TEM results of the 2.0 % K promoted catalyst showed that a thick amorphous carbon deposited around the surface of the catalyst particles; this massive build-up of carbon growth that occurred with synthesis time led to the deactivation of the catalyst. Similar findings were observed by Dwyer [58], who reported that potassium promotion of an unsupported iron catalyst causes an order of magnitude loss in CO conversion and an increase in high molecular weight material while inducing the growth of a 2-mm-thick hydrocarbonaceous layer on the catalyst surface. This layer was not present in the unpromoted catalyst. They confirmed carbon layer formation by using X-ray photoelectron spectroscopy measurements. Similarly, de Smit et al. [59] reported that a catalyst containing $\theta\text{-Fe}_3\text{C}$ and amorphous carbide phases showed a lower activity and selectivity, mainly due to the buildup of carbonaceous deposits on the catalyst surface, suggesting that amorphous phases and the resulting textural properties play an important role in determining catalyst performance. Lohitharn and Goodwin [60] reported that addition of potassium at relatively low concentrations promoted the activity of the catalysts, while the activity of the catalysts declined with excess addition of K probably in large part due to an increased amount of carbon deposited via the Boudouard reaction. The intrinsic site activities (TOF_{ITK}) of all the Fe catalysts determined using SSITKA were essentially identical, regardless of the concentration of added K. This indicates that addition of K to unpromoted Fe catalysts did not greatly affect the activity of the active sites. Rather, the higher retention of catalyst activities observed for the K promoted Fe catalysts were due primarily to the maintenance of the number of active surface intermediates leading to hydrocarbon products.

The data for the unpromoted and K promoted catalysts show that a carbide phase (in this case, the $\chi\text{-Fe}_5\text{C}_2$ phase) is necessary to obtain high activity for the FTS reaction. For the unpromoted catalyst, the decrease in catalytic activity parallels the amount of iron carbide in the catalyst

and this clearly shows that the carbide is a significantly more active catalyst than Fe_3O_4 . A simple relationship of activity to the carbide phase would be misleading. Based only on the catalytic activity and the iron carbide phases present, one would conclude that $\chi\text{-Fe}_5\text{C}_2$ is catalytically active and that $\delta\text{-Fe}_2\text{C}$ is not, or at least much less, active. This would be an incorrect conclusion since the formation of significant amounts of carbon surrounds most of the catalyst particles. This carbon mass therefore limits the contact of the gaseous reactants with the catalyst surface so that a reliable determination of the relative activities of different iron carbides cannot be made by just considering the type of iron carbide phase that is present.

5 Conclusions

The activity and stability of the catalysts pass through a maximum for the 100Fe:0.5K catalyst and further increases in potassium loading decrease the stability. CO-TPR results reveal that increasing the potassium loading enhances the carburization rate of the catalysts. Mössbauer spectroscopy results reveal that for the unpromoted catalyst, the deactivation of the catalyst was due to oxidation of the catalyst, due to the formation of Fe_3O_4 with increasing TOS, and the corresponding $\chi\text{-Fe}_5\text{C}_2$ phase decreased. For the 100Fe:0.5K catalyst, the presence of the $\chi\text{-Fe}_5\text{C}_2$ phase was still high even after ~ 280 h on stream. For the more highly loaded potassium (1 and 2K) catalysts, the iron carbide phase ($\chi\text{-Fe}_5\text{C}_2$) gradually decreased, whereas the other iron carbide phase ($\delta\text{-Fe}_2\text{C}$) steadily increased and the corresponding magnetite phase remained relatively unchanged. TEM analyses demonstrated that with increasing the potassium loading, the formation of carbon around the catalyst surface gradually increased with time on stream. The results of this study clearly indicate that the presence of an iron carbide phase (in the present case, $\chi\text{-Fe}_5\text{C}_2$) is necessary to obtain high FTS activity. Based on the catalytic activity and the iron carbide phases present, $\delta\text{-Fe}_2\text{C}$ appears to be less active as a FTS catalyst. This would be an incorrect conclusion, since the formation of significant amounts of carbon surrounds most, or all, of the catalyst particles. This carbon mass therefore limits the contact of gaseous reactants with the catalyst so that a reliable determination of the relative activities of different iron carbides cannot be made. The selectivity of these catalysts to higher average molecular weight FTS products increased with increasing potassium loading, which is likely due to an enhancement of CO coverage and suppression of H_2 surface coverage in the presence of potassium.

Acknowledgments This work was supported by a grant from the University of Wyoming (contract number 1001541-Davis) and by the Commonwealth of Kentucky.

References

- Keyvanloo K, Mardkhe MK, Alam TM, Bartholomew CH, Woodfield BF, Hecker WC (2014) *ACS Catal* 4:1071
- Anderson RB (1956) Catalysts for Fischer–Tropsch synthesis. In: Emmett PH (ed) *Catalysis*, vol IV. Van Nostrand-Reinhold, New York, p 29
- Kölbl H (1960) Kalium als struktureller und Energetischer Promotor in Eisenkatalysatoren. In: *Actes du Deuxieme Congress International de Catalyse*, vol. II. Technip, Paris, p 2075
- Kölbl H, Giehring H (1963) *Brennstoff-Chem* 44:343
- Anderson RB (1984) *The Fischer-Tropsch synthesis*. Academic Press, Orlando
- Anderson RB, Sekigman B, Schulz JF, Elliot MA (1952) *Ind Eng Chem* 44:391
- Dry ME, Oosthuizen GJ (1968) *J Catal* 11:18
- Dry ME, Shingles T, Boshoff L, Oosthuizen GJ (1969) *J Catal* 15:190
- Amelse JA, Butt JB, Schwartz LH (1978) *J Phys Chem* 82:558
- Benziger J, Madix R (1980) *Surf Sci* 94:119
- Dry ME (1981) *The Fischer–Tropsch synthesis*. In: Anderson JR, Boudart M (eds) *Catalysis science and technology*, vol 1. Springer, New York, p 159
- Pennline HW, Zarochak MF, Stencel JM, Diehl JR (1987) *Ind Eng Chem Res* 26:595
- Bukur DB, Mukesh DS, Patal A (1990) *Ind Eng Chem Res* 29:194
- Milburn DR, Chary KVR, Davis BH (1996) *Appl Catal A* 144:133
- Kündig W, Bommel H, Constabaris G, Lindquist RH (1966) *Phys Rev* 142:327
- Jiang M, Koizumi N, Yamada M (2000) *Appl Catal A* 204:58
- Dictor RA, Bell AT (1986) *J Catal* 97:121
- Rankin JL, Bartholomew CH (1986) *J Catal* 100:533
- Arakawa H, Bell AT (1983) *Ind Eng Chem Process Des Dev* 22:97
- Miller DG, Moskovits M (1988) *J Phys Chem* 92:6081
- Pichler H (1952) Twenty-five years of synthesis of gasoline by catalytic conversion of carbon monoxide and hydrocarbon. In: Frankeberg WG, Komarewsky VI, Rideal EK (eds) *Advances in catalysis*, vol 4. Academic Press, New York, p 271
- Pendyala VRR, Graham UM, Jacobs G, Hamdeh HH, Davis BH (2014) *ChemCatChem* 6:1952
- Eliason SA, Bartholomew CH (1999) *Appl Catal A* 186:229
- Nakhaei Pour A, Shahri SMK, Zamani Y, Irani M, Tehrani S (2008) *J Nat Gas Chem* 17:242
- Sarkar A, Seth D, Dozier AK, Neathery JK, Hamdeh HH, Davis BH (2007) *Catal Lett* 117:1
- Anderson RB (1956) In: Emmett PH (ed) *Catalysis*, vol 4. Reinhold, New York, p 1
- Ning W, Koizumi N, Chang H, Mochizuki T, Itoh T, Yamada M (2006) *Appl Catal A* 312:35
- Li S, O'Brien RJ, Meitzner GD, Hamdeh H, Davis BH, Iglesia E (2001) *Appl Catal A* 219:215
- Niemantsverdriet JW, van der Kraan AM, van Dijk WL, van der Baan HS (1980) *J Phys Chem* 84:3363
- Loaiza-Gil A, Fontal B, Rueda F, Mendiola J, Casanova R (1999) *Appl Catal A* 177:193
- Yong Y, Xiang HW, Tian L, Wang H, Zhang CH, Tao ZC, Xu YY, Zhong B, Li YW (2005) *Appl Catal A* 284:105

32. Pendyala VRR, Jacobs G, Hamdeh HH, Shafer WD, Sparks DE, Hopps S, Davis BD (2014) *Catal Lett*. doi:10.1007/s10562-014-1302-9
33. Ribeiro MC, Jacobs G, Davis BH, Cronauer DC, Kropf AJ, Marshall CL (2010) *J Phys Chem C* 114:7895
34. Ribeiro MC, Jacobs G, Pendyala R, Davis BH, Cronauer DC, Kropf AJ, Marshall CL (2011) *J Phys Chem C* 115:4783
35. Jacobs G, Sarkar A, Davis BH, Cronauer DC, Kropf AJ, Marshall CL (2009) In: Davis BH, Occelli ML (eds) *Advances in Fischer-Tropsch synthesis, catalysts and catalysis*. Taylor & Francis, Boca Raton, pp 119–146
36. Zhang CH, Yang Y, Teng BT, Li TZ, Zheng HY, Xiang HW, Li YW (2006) *J Catal* 237:405
37. Li S, Li A, Krishnamoorthy S, Iglesia E (2001) *Catal Lett* 77:197
38. Jin Y, Datye AK (2000) *J Catal* 196:8
39. Shultz JF, Hall WK, Dubs TA, Anderson RB (1956) *J Am Chem Soc* 78:282
40. Rao KRPM, Huggins FE, Mahajan V, Huffman GP, Rao VUS, Bhatt BL, Bukur DB, O'Brien RJ (1995) *Top Catal* 2:71
41. Mansker LD, Jin Y, Bukur DB, Datye AK (1999) *Appl Catal A* 186:277
42. Li S, Meitzner GD, Iglesia E (2001) *J Phys Chem B* 105:5743
43. Hilmen AM, Lindvag OA, Bergene E, Schanke D, Eri S, Holmen A (2001) *Stud Surf Sci Catal* 136:295
44. Pendyala VRR, Jacobs G, Luo M, Davis BH (2013) *Catal Lett* 143:395
45. Lang ND, Williams AR (1976) *Phys Rev Lett* 37:212
46. Luo M, O'Brien RJ, Bao S, Davis BH (2003) *Appl Catal A* 239:111
47. Schulz H (1999) *Appl Catal A* 186:3
48. Yang Y, Xiang HW, Xu YY, Bai L, Li YW (2004) *Appl Catal A* 266:181
49. Zhang YQ, Sirimanothan N, O'Brien RJ, Hamdeh H, Davis BH (2001) *Stud Surf Sci Catal* 139:125
50. Raje AP, O'Brien RJ, Xu L, Davis BH (2007) *Stud Surf Sci Catal* 111:527
51. Butt JB (1990) *Catal Lett* 7:61
52. Hwang JS, Jun KW, Lee KW (2001) *Appl Catal A* 208:217
53. McDonald MA, Storm DA, Boudart M (1986) *J Catal* 102:386
54. Dry ME (1990) *Catal Lett* 7:241
55. Duvenhage DJ, Coville NJ (2006) *Appl Catal A* 298:211
56. Pendyala VRR, Jacobs G, Mohandas JC, Luo M, Hamdeh H, Ji Y, Ribeiro MC, Davis BH (2010) *Catal Lett* 140:98
57. Bukur DB, Okabe K, Rosynek MP, Li C, Wang D, Rao KRPM, Huffman GP (1995) *J Catal* 155:353
58. Dwyer DJ (1984) *Preprints - ACS Div Petrol* 29:715
59. de Smit E, Cinquini F, Beale AM, Safonova OV, van Beek W, Sautet P, Weckhysen BM (2010) *J Am Chem Soc* 132:14928
60. Lohitharn N, Goodwin JG Jr (2008) *J Catal* 260:7